Journal of Hazardous Materials 185 (2011) 430–441

Contents lists available at ScienceDirect

Journal of Hazardous Materials

journal homepage: www.elsevier.com/locate/jhazmat

Competitive biosorption of azo dyes from aqueous solution on the templated crosslinked-chitosan nanoparticles

Chia-Yun Chen, Jen-Chao Chang, Arh-Hwang Chen*

Department of Chemical and Materials Engineering, Southern Taiwan University, Tainan 710, Taiwan, ROC

ARTICLE INFO

Article history:
Received 25 March 2010
Received in revised form 8 July 2010
Accepted 16 September 2010
Available online 22 September 2010

Keywords:
Biosorption
Azo dye
Templated crosslinked-chitosan nanoparticle
Competition
Regeneration

ABSTRACT

The nanoparticles of templated crosslinked chitosan, ECH-RB5 and ECH-3R, were prepared through the imprinting process using Remazol Black 5 (RB5) and Remazol Brilliant Orange 3R (3R) dyes, respectively, as templates and ECH as a crosslinker. The nanoparticles exhibited significantly higher adsorption capacities of the dyes than other nanoparticles formed without a dye template and with three crosslinkers (ECH, GLA, and EGDE). The adsorption of the dyes on the nanoparticles was affected by the initial pH, dye concentration, and temperature. The results were in accordance with the second-order and the Langmuir adsorption models. Meanwhile, the *E* values of the dyes calculated using the Dubinnin-Radushkevich model revealed that the adsorption process may be due to the dual nature of the process, physisorption and chemisorption, and that adsorption was predominant in the chemisorption process. The adsorption processes in the nanoparticles were spontaneous and exothermic. Moreover, competition adsorption through analysis of the intraparticle diffusion model apparently favored the 3R dye more than the RB5 dye on the nanoparticles in mixture solution B. The nanoparticles for the adsorption of the dyes were regenerated efficiently through the alkaline solution and were then reused for dye removal.

1. Introduction

Various kinds of synthetic dyestuffs are found in the effluents of wastewater in the dyestuff, textile, leather, paper, and plastic industries. Unfortunately, the dyes, particularly azo dyes with aromatic structures, are comprised of recalcitrant molecules. Thus, azo dyes are resistant to aerobic digestion and are stable in oxidizing agents. Moreover, most of these dye wastes are toxic and may be carcinogenic. The immense volume of aromatic structures present in dye molecules makes wastewater treatment through a biological process tedious and ineffective. This results in the release of the materials into the environment [1]. Numerous studies have been conducted on the different viable techniques in eliminating dyes in wastewater. The conventional treatment methods for dye removal, such as chemical coagulation, activated sludge, biodegradation, oxidation, membrane separation, adsorption, and photodegradation, have been extensively explored [1,2]. Among the physical and chemical processes, the adsorption procedure is effective in producing high-quality effluent without the formation of harmful substances [3,4]. However, low-cost adsorbents with high adsorption capacities are still being developed to reduce the adsorbent dose and minimize the problem of disposal. Significant attention has been directed toward various biosorbent materials, such as fungal or bacterial biomass and biopolymers, which may be obtained in significant quantities and are nontoxic to nature [1].

Chitosan, a type of natural aminopolysaccharide derived from chitin, is utilized as one of the most popular adsorbents that eliminate metal ions, dyes, and proteins from aqueous solutions. Moreover, chitosan has been widely used in waste treatment applications [5–9]. However, the amino groups of chitosan are fully protonated at around pH 3.0, and the positively charged polymer chains disintegrate in the solution. This results in the dissolution in an acidic medium. Hence, the crosslinking reactions of chitosan with various crosslinkers have been studied to improve its chemical stability in any acidic media for the extraction of dyes from industrial wastewater. Chiou et al. studied the adsorption of different dyes onto chitosan beads crosslinked with epichlorohydrin (ECH) [10–13]. Hu et al. [4] and Du et al. [14] worked on the biosorption of Acid Green 27 and ecosin Y dyes, respectively, on chitosan nanoparticles prepared by ionic gelation with sodium tripolyphosphate (TPP). Rosa et al. utilized quaternary chitosan salt crosslinked with glutaraldehyde (GLA) for the adsorption of Reactive Orange 16 dye [15], whereas Elwakeel prepared magnetic chitosan resins for the elimination of Reactive Black 5 dye [16]. Chen et al. also prepared glutaraldehyde-crosslinked-chitosan microparticles for the biosorption of Remazol Black 5 (RB5) and Remazol Brilliant Orange (3R) dyes and templated epichlorohydrin-crosslinked-chitosan microparticles for the adsorption of BR5 dyes [17,18]. Although

* Corresponding author. Tel.: +886 6 2533131x6937; fax: +886 6 2432846.
E-mail address: chenah@ms12.hinet.net (A.-H. Chen).

0304-3894/$ – see front matter.
doi:10.1016/j.jhazmat.2010.09.051

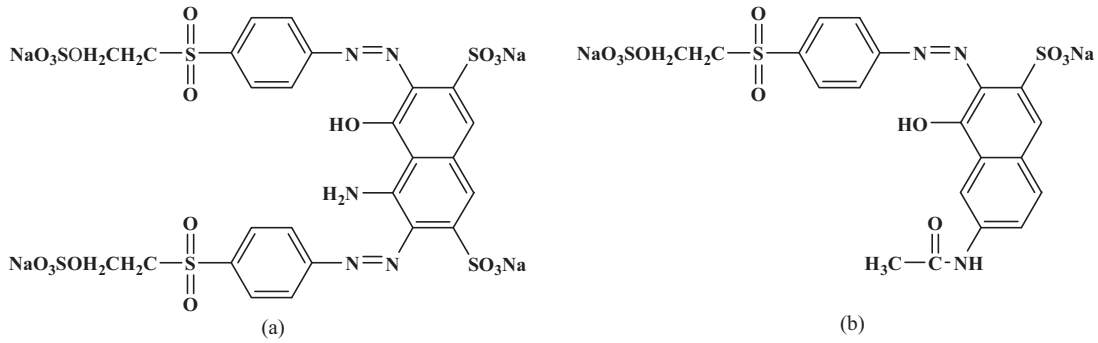

Fig. 1. The structures of (a) Remazol Black 5 and (b) Remazol Brilliant Orange 3R.

the crosslinking method may enhance the resistance of chitosan against acids, the process may reduce its adsorption capacity for dyes. This may be attributed to the fact that the crosslinking reaction decreases the amount of amino and hydroxyl groups, which are expected to play a great part in the adsorption process.

To overcome this dilemma, this study was conducted to prepare templated crosslinked-chitosan nanoparticles using the imprinting method. The nanoparticles were characterized by determining size distributions, zeta potentials, SEM images, Fourier transform infrared (FTIR), and solid state ^{13}C nuclear magnetic resonance (^{13}C NMR) spectra. Afterward, the nanoparticles were used in the competition biosorption of two azo dyes, RB5 and 3R, in an aqueous solution. pH influence, kinetics, equilibrium, thermodynamics, competition, intraparticle diffusion, and regeneration were also examined for a more in-depth comparison of the experimental results. This information is expected to be valuable for further applications in the treatment of waste effluents from the dye industry.

2. Materials and methods

2.1. Chemicals

Chitosan was purchased from Sigma–Aldrich Co., USA. Chitosan was hydrolyzed with NaOH to yield a deacetylation percentage of approximately 90% using the FTIR methods [19]. The average molecular weight was 690,000 as measured through the viscometric method [20]. RB5 (M_w = 991.82 g/mol; λ_{max} = 597 nm), 3R (M_w = 617.54 g/mol; λ_{max} = 494 nm), ECH, GLA, ethylene glycol diglycidyl ether (EGDE), and TPP with 55%, 50%, 99%, 50%, 50%, and 85% purities, respectively, were purchased from Sigma–Aldrich Co., USA. No further purification of the reagents was performed. Stock solutions of the dyes (2.0×10^4 mg/L) were prepared by dissolving RB5 or 3R dyes in distilled water. The RB5 and 3R dye structures are shown in Fig. 1.

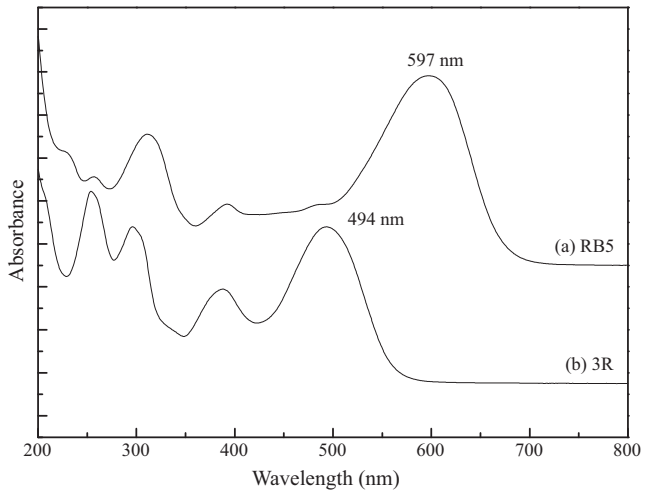

Fig. 2. UV/visible spectra of the RB5 and 3R dyes.

2.2. Preparation

A solution with 50 mg of chitosan dissolved into a 50 mL aqueous solution of acetic acid (0.5%, v/v) was prepared. A 5.0 mL aqueous solution of RB5 dye (8.7 mg) was added, and the mixture was stirred for 30 min. A 5.0 mL aqueous solution of ECH was added dropwise, and the mixture was stirred for 2 h at 50 °C. Using a syringe, 30 mL of 1.45% TPP solution was slowly dropped into the chitosan solution by mechanical stirring (1200 rpm) to obtain a milky emulsion. The resulting emulsion was frozen at −4 °C and then thawed in the atmosphere to produce nanoparticle precipitates, which were collected using a centrifuge. Finally, the nanoparticle precipitates were stirred with a pH 14.0 NaOH solution to remove the dye. This stage was monitored by a UV/visible spectrophotometer (Shimadzu UV-2401 PC). The process was followed by collecting the precipitates with a centrifuge and by intensive washing of the nanoparticle precipitates with distilled water to remove any unreacted ECH. The nanoparticle precipitates were re-suspended in distilled water for characterization and were directly used in the adsorption study.

The size distribution and zeta potential of the nanoparticles were determined using a Zetasizer 3000HS. FTIR spectra were obtained using a PerkinElmer Spectrum One FTIR spectrometer. The solid state ^{13}C nuclear magnetic resonance spectra of the materials were obtained on a Brucker Advance 400 NMR spectrometer. The scanning electron microscopy (SEM) photomicrographs of the nanoparticles were taken using a Jeol JSM-6700F SOP SEM.

2.3. Adsorption of azo dyes

The nanoparticles prepared from a 0.5 molar ratio of crosslinker/chitosan, with or without the RB5 or 3R dyes as templates and with three different crosslinkers (ECH, GLA and EGDE), were studied to determine the adsorption capacity of the RB5 and 3R dyes. This process was conducted by adding 10 mL of each kind of the nanoparticles (9 mg/mL) into a 10 mL of 6.0 mg/mL dye solution, then adjusting to pH 3.0 using HCl or NaOH solutions while stirring at 30 °C for 120 h. The mixture solution was centrifuged to remove adsorbents. The filtrate was adjusted to a pH level of 6.0 using HCl or NaOH solutions, and then diluted to 50 mL. The dye concentration was measured using a UV/visible spectrophotometer at 597 nm for the RB5 dye and at 494 nm for the 3R dye, whereas the adsorption capacity (Q) was calculated using Eq. (1):

$$Q = \frac{(C_i - C_f)V}{W} \quad (1)$$

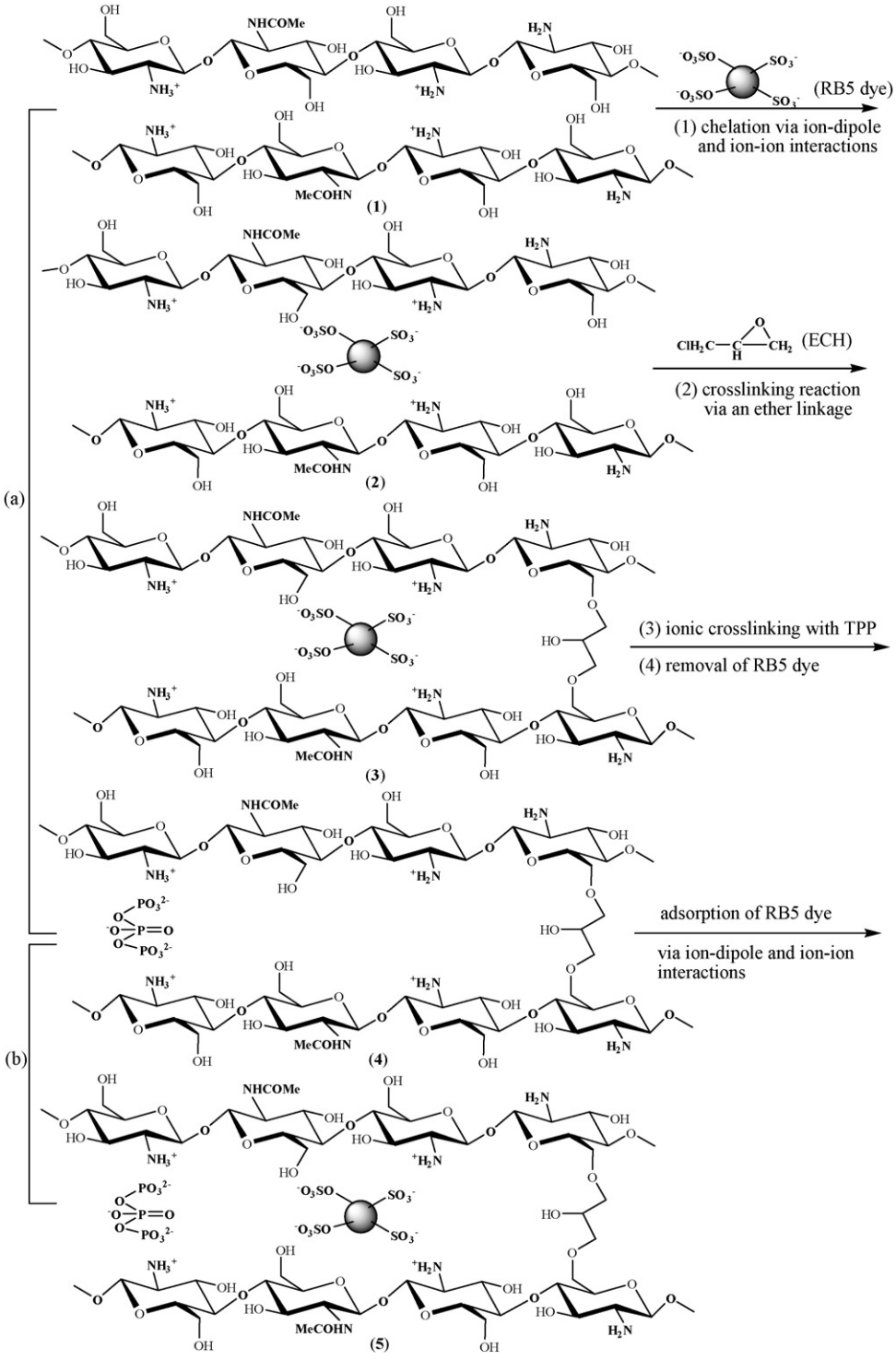

Fig. 3. Schematic representation for (a) preparation of the templated crosslinked-chitosan nanoparticles with epichlorohydrin and (b) the adsorption of dyes.

where C_i is the initial concentration of dye (mg/mL); C_f is the final concentration of dye (mg/mL); V is the volume of dye solution (mL); and W is the weight of the nanoparticles (g) used.

2.4. Batch kinetics

The adsorption kinetics of the RB5 and 3R dyes on the nanoparticles was carried out in a batch process. The variable parameters were studied, including the initial pH values, initial concentrations of dye, and temperatures. In each test, 10 mL of the nanoparticles (9 mg/mL) was added into 10 mL of aqueous solution of the dye with a known concentration. Whenever necessary, the pH value was adjusted with diluted NaOH or HCl solutions. Then 0.1 mL aliquots of the solution were added to 10 mL distilled water at different time intervals. The mixture solution was centrifuged to remove adsorbents. The filtrate was adjusted to pH 6.0 and then diluted to 25 mL. The dye concentrations were measured using a UV/visible spectropho-

tometer. The amount of adsorption was calculated using Eq. (1).

To measure the rate-controlling and mass transfer mechanism, kinetic data were correlated to linear forms of the first-order equation (2):

$$\ln(Q_e - Q_t) = \ln Q_e - k_1 t, \quad (2)$$

and the second-order equation (3):

$$\frac{t}{Q_t} = \frac{1}{(k_2 Q_e^2)} + \frac{t}{Q_e}. \quad (3)$$

where Q_e and Q_t are the adsorption capacities of dye (mg/g) at equilibrium and at a given time t, respectively; and k_1 (min^{-1}) and k_2 (g/(mg min)) are the first-order and the second-order rate constants, respectively. According to Eq. (2), the plot of $\ln(Q_e - Q_t)$ versus t yields a straight line with a slope of $-k_1$ and an intercept of $\ln Q_e$. In Equation (3), the plot of t/Q_t versus t gives a straight line with a slope of $1/Q_e$ and an intercept of $1/(k_2 Q_e^2)$.

2.5. Batch equilibrium

Equilibrium studies were conducted by adding 10 mL of the nanoparticles (9 mg/mL) into 10 mL of the initial dye concentrations within the range of 1.0–20.0 mg/mL, adjusting to pH 3.0 using HCl or NaOH solutions, and then stirring for 120 h at 30 °C. The mixture solution was centrifuged to remove adsorbents. The filtrate was adjusted to pH 6.0 and then diluted to 50 mL. The dye concentrations were measured using a UV/visible spectrophotometer. In accordance with Eq. (1), the amount of adsorption was calculated based on differences in concentration in the aqueous solution before and after adsorption, as well as on the weight of the microparticles.

2.6. Competition study

Assuming there is no interaction between the RB5 and 3R dyes, the total absorbance of a mixture dye solution is equal to the summation of the absorbance of each dye, which is represented by Eq. (4). The concentration of each dye in a mixture solution can be calculated using Eqs. (5) and (6).

$$A_\lambda = A_{RB5} + A_{3R} \quad (4)$$

$$A_{\lambda 1} = \varepsilon_{1RB5} L C_{RB5} + \varepsilon_{13R} L C_{3R} \quad (5)$$

$$A_{\lambda 2} = \varepsilon_{2RB5} L C_{RB5} + \varepsilon_{23R} L C_{3R} \quad (6)$$

where A_λ, $A_{\lambda 1}$ and $A_{\lambda 2}$ are the absorbance of UV/visible spectrometer at wavelength λ, λ_1 and λ_2, respectively; A_{RB5} and A_{3R} are the absorbance of RB5 and 3R at wavelength λ, respectively; ε_{1RB5} and ε_{2RB5} are the molar absorptivities of pure RB5 at wavelength λ_1 and λ_2, respectively; ε_{13R} and ε_{23R} re the absorbance coefficients of pure 3R at wavelength λ_1 and λ_2, respectively; C_{RB5} and C_{3R} are the concentrations of RB5 and 3R in the mixture solution, respectively; L is the cell with (1 cm); and λ_1 (597 nm) and λ_2 (494 nm) are the wavelengths of maximum absorbance for RB5 and 3R, respectively, in Fig. 2. The concentrations of C_{RB5} and C_{3R} are calculated from Eqs. (5) and (6). The adsorption capacity of each dye in the mixture solution can then be obtained.

3. Results and discussion

3.1. Characterization and azo dye adsorption

The nanoparticles were prepared using the imprinting process through the following steps: (1) chelation of the RB5 and 3R dyes as templates into chitosan through ion–dipole and ion–ion interactions, (2) crosslinking reaction of chitosan with three crosslinkers (ECH, GLA, and EGDE), (3) nanoparticle formation of chitosan through ionic crosslinking with TPP, and (4) removal of the dye template molecules with NaOH solution, as shown in Fig. 3(a) for the ECH-RB5 nanoparticles through an ether linkage. The nanoparticles were revealed to be insoluble in distilled water, alkaline medium, and even in acidic medium (pH 1.0). Fig. 4(a) and (b) shows the typical size distributions and zeta potential profiles of the ECH-RB5 nanoparticles with a mean diameter of 191.6 nm and a zeta potential of +14.4 mV, respectively. Other nanoparticles prepared through three crosslinkers, namely, ECH, GLA, and EGDE, with or without a dye template, had mean diameters ranging from 170.2 to 210.6 nm and zeta potential values ranging from +12.4 to +16.4 mV. The positive charge of the zeta potential suggested that the nanoparticles were stabilized by the hydrogen bond between

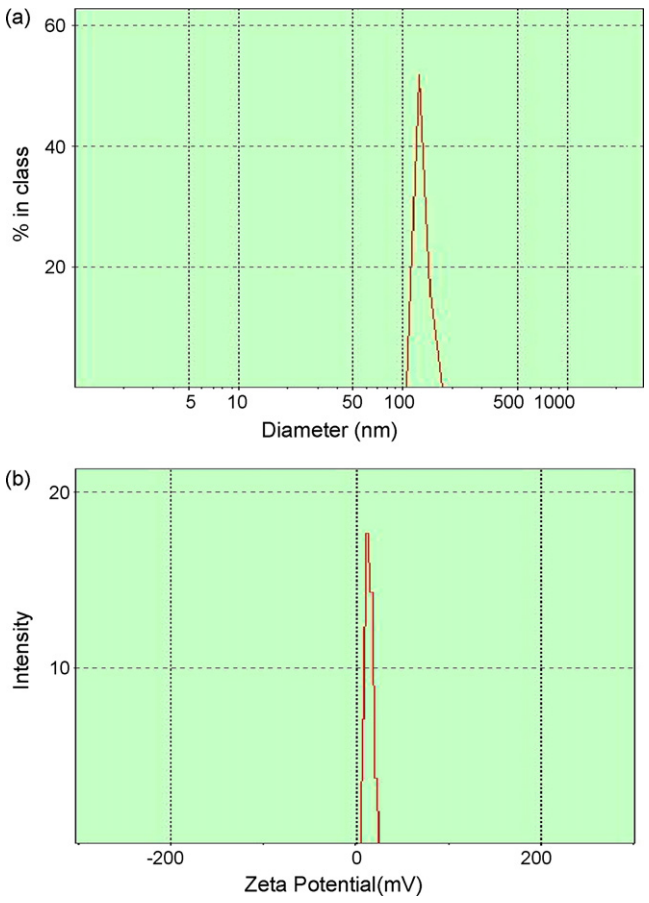

Fig. 4. (a) Size distribution and (b) zeta potential for the ECH-RB5 nanoparticles.

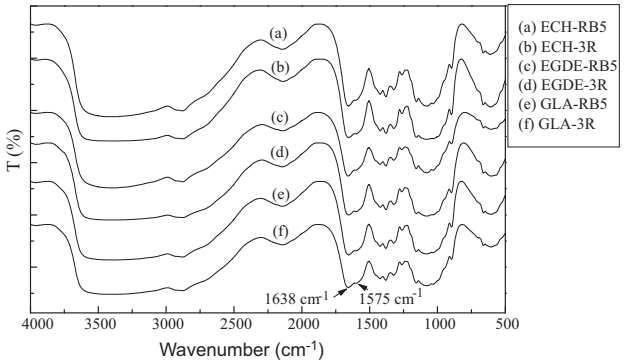

Fig. 5. FTIR spectra of the templated crosslinked-chitosan nanoparticles prepared through three crosslinkers with the RB5 or 3R dyes as templates.

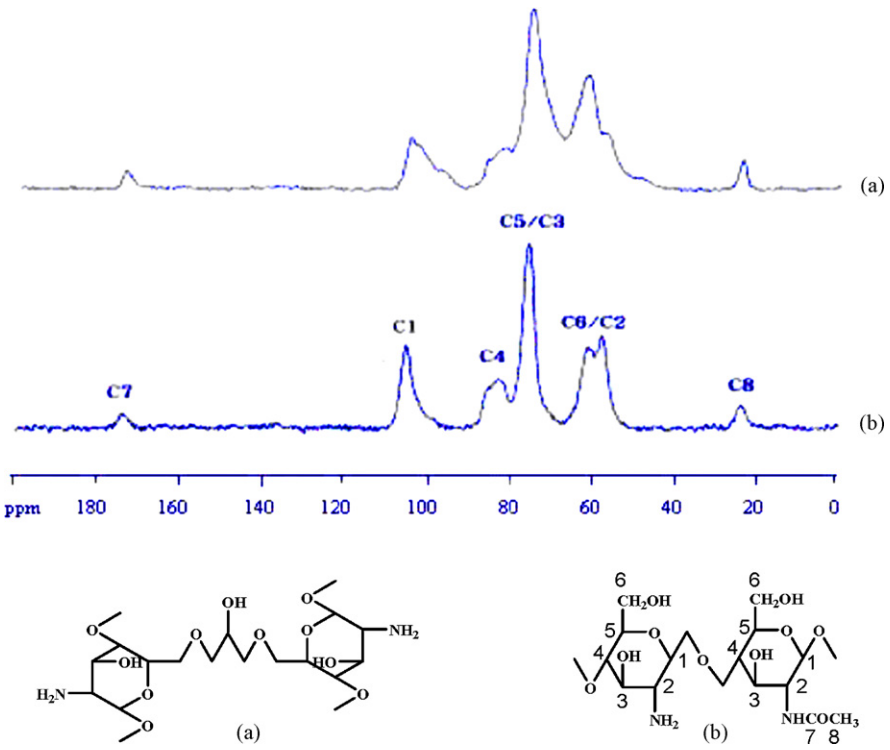

Fig. 6. Solid state ^{13}CNMR of (a) ECH-RB5 nanoparticles and (b) chitosan with a partial acetylation.

the amino and hydroxyl groups of the chitosan and the hydroxyl group and oxygen atom of water [4]. The SEM image of dry ECH-RB5 nanoparticles on a silicon wafer showed that the nanoparticles had a diameter of approximately 90 nm due to loss of water. Fig. 5 showed the FTIR spectra of the templated nanoparticles prepared through ECH, GLA, and EGDE with the RB5 or 3R dyes as templates. The nanoparticles showed an absorption peak for amide C=O and/or imine C=N stretching vibrations at 1638 cm^{-1}, which were dependent on the crosslinker used, and an absorption peak of 1575 cm^{-1}, which accounted for the ionic interaction between the positively charged amino groups of crosslinked chitosan and the negatively charged groups of triphosphate ($P_3O_{10}^{5-}$) [21]. In Fig. 6, compared with that of chitosan, the solid state ^{13}C NMR of the ECH-RB5 nanoparticles exhibited three additional peaks at 61.6, 85.0, and 97.6 ppm due to the exit of the –O–CH_2–CHOH–CH_2–O– linkage between two chitosan molecules.

The adsorption capacities of the two azo dyes, RB5 and 3R, on the nanoparticles prepared from three crosslinkers (ECH, GLA, and EGDE) with or without the RB5 or 3R dyes as templates were conducted at 6.0 mg/mL initial dye concentration with an initial pH of 3.0 and a temperature of 30 °C for 120 h. The adsorption processes may involve ion–dipole and ion–ion interactions between sulfonate and sulfate anions of the dye molecules and the hydroxyl and protonated amino groups of chitosan molecules (Fig. 3(b)). The results showed that the adsorption capacities of the RB5 and 3R dyes on the templated nanoparticles were significantly higher than those of the chitosan nanoparticles and the crosslinked nanoparticles formed without a dye template. In addition, the ECH-RB5 nanoparticles that formed with the RB5 dye as template showed that the adsorption capacity of the RB5 dye was much higher than that of the 3R dye. The ECH-3R nanoparticles that formed with the 3R dye as template also yielded similar results. Moreover, the adsorption capacity of the RB5 dye on the ECH-RB5 nanoparticles and that of the 3R dye on the ECH-3R nanoparticles were higher than the adsorption capacities of the two dyes on other nanoparticles. Therefore, the technique for the preparation of templated nanoparticles yielded a higher adsorption capacity and a more efficient adsorption of dyes in an aqueous solution.

3.2. Adsorption kinetics

Fig. 7(a) and (b) presented the influences of the initial pH values from 1.0 to 12.0 for the adsorption capacities of the RB5 and 3R dyes on the ECH-RB5 and the ECH-3R nanoparticles, respectively, at an initial dye concentration of 8.0 mg/mL and at a temperature of 30 °C for 72 h. The pH values were monitored before and after the adsorption of the dyes with a pH difference of only 0.1 to 0.2. The adsorption capacities of the RB5 and 3R dyes on the ECH-RB5 nanoparticles increased 40 times from 148 to 6080 mg/g and 39 times from 128 to 5078 mg/g, respectively, as the initial pH of the solution decreased from 12.0 to 1.0. In addition, the adsorption capacities of the RB5 and 3R dyes on the ECH-3R nanoparticles increased 49 times from 92 to 4626 mg/g and 20 times from 306 to 6292 mg/g, respectively, as the initial pH of the solution decreased from 12.0 to 1.0. This may be ascribed to the fact that at a lower pH solution, more protons are available to protonate the amino groups of chitosan to form $–NH_3^+$ groups. This increases the electrostatic attraction between the anionic groups ($–SO_3^-$ and $–OSO_3^-$) of the dye and the protonated amino group ($–NH_3^+$) of chitosan, causing an increase in dye adsorption [17,22]. Fig. 8(a) showed the adsorption kinetics of the RB5 dye in the ECH-RB5 nanoparticles that had a 6.0 mg/mL initial dye concentration, a temperature of 30 °C, and initial pH values of 3.0, 4.0, and 6.0. The rapid initial rates of adsorption on the nanoparticles showed a remarkable increase during the first 12 h, and the nanoparticles gradually approached the adsorption limit after 60 h. At the same time, the adsorption kinetics of the 3R dye on the ECH-3R nanoparticles had the same results. This may be ascribed to the increase in the number of vacant sites that are usually available, resulting in an increased concentration gradient between the sorbate in the solution and that on the adsorbent

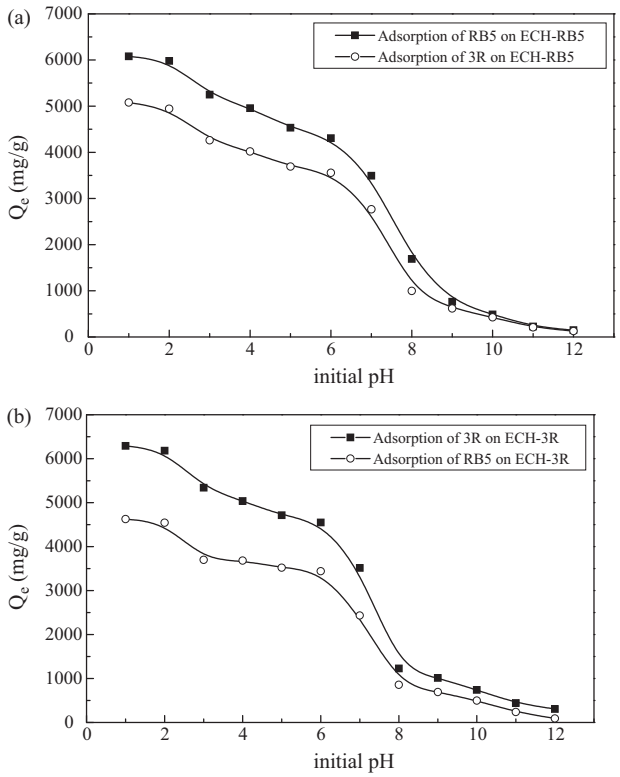

Fig. 7. The effect of pH for adsorption capacities of the RB5 and 3R dyes on the nanooparticles: (a) ECH-RB5 and (b) ECH-3R, at an initial dye concentration of 8.0 mg/mL and at a temperature of 30 °C for 72 h with different initial pHs.

surface. In time, the concentration gradient is reduced due to the adsorption of the dye molecules onto the vacant sites, leading to decreased adsorption during the later stages [23].

Fig. 8(b) showed the effects of the initial dye concentration (2.0, 4.0, and 6.0 mg/mL) in the adsorption kinetics of the RB5 dye on the ECH-RB5 nanoparticles at pH 3.0 and at 30 °C. As the initial concentrations of the RB5 and 3R dyes increased from 2.0 to 6.0 mg/mL, the adsorption capacities of the RB5 dye on the ECH-RB5 nanoparticles and of the 3R dye on the ECH-3R nanoparticles increased by 138% (from 2125 to 5057 mg/g) and by 141% (from 1994 to 4811 mg/g). However, the removal efficiencies of the RB5 and 3R dyes decreased from 100% to 79.3% and from 100% to 80.5%, respectively, as the initial dye concentration increased from 2.0 to 6.0 mg/mL. This may be attributed to the fact that compared with the available surface area, the ratio of the initial moles of dye is low at minimum initial concentrations; therefore, the subsequent fractional adsorption becomes independent of the initial concentration. However, at high concentrations, the available adsorption sites are fewer than the moles of the dye present; hence, the percentage of dye removal is dependent on the initial dye concentration [23].

The effects of temperature (30, 40, and 50 °C) on the adsorption kinetics of the RB5 dye in the ECH-RB5 nanoparticles at 6.0 mg/mL initial dye concentration and pH 3.0 were shown in Fig. 8(c). The adsorption capacities of the RB5 dye on the ECH-RB5 nanoparticles increased along with temperature during the initial 44 h and were close to each other at 120 h. At the same time, the adsorption capacities of the 3R dye on the ECH-3R nanoparticles yielded similar results. Tables 1 and 2 presented the rate constants for the RB5 dye on ECH-RB5 and the 3R dyes on the ECH-3R nanoparticles, respectively, with a different initial pH, initial dye concentrations, and temperatures that were calculated by the first-order and second-order kinetic models. The correlation coefficients (R^2) of the second-order adsorption model exhibited higher values than those of the first-order kinetics. In addition, the calculated equilibrium adsorption capacities ($Q_{e,cal}$) fitted the experimental Q_e values well. This suggested that the second-order adsorption mechanism was predominant and that the overall rate of the dye adsorption process appeared to be controlled by the chemical process [11].

3.3. Adsorption equilibrium

The adsorption isotherms of the RB5 dye on the ECH-RB5 nanoparticles and the 3R dye on the ECH-3R nanoparticles were at pH 3.0 and at 30 °C for 120 h with different equilibrium dye concentrations (Fig. 9). The steep initial isotherm slopes for the RB5 dye on the ECH-RB5 nanoparticles and the 3R dye on the ECH-3R nanoparticles with peak adsorption capacities of 5497 and 5123 mg/g, respectively, were observed under these conditions.

The adsorption isotherm data were studied using three models: Langmuir isotherm equation (7) [24],

$$\frac{C_e}{Q_e} = \frac{C_e}{Q_m} + \frac{1}{(Q_m K_L)}, \quad (7)$$

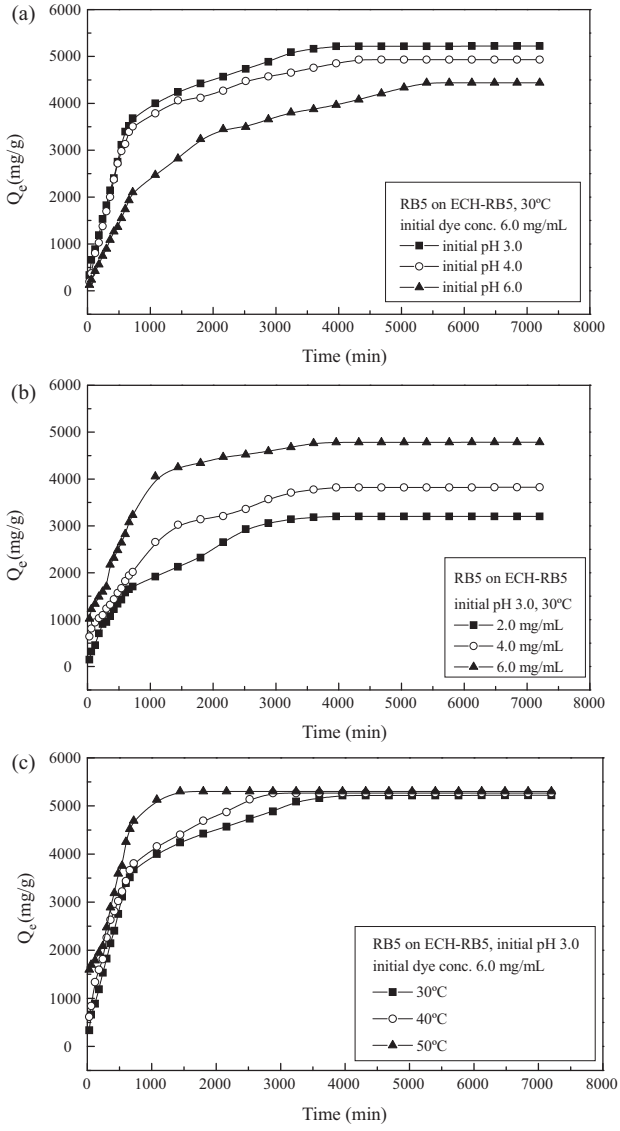

Fig. 8. Absorption kinetics of the RB5 dye on the ECH-RB5 nanoparticles: (a) different initial pH solutions, (b) different initial concentrations of dye and (c) different temperatures.

Table 1
The first-order and second-order adsorption rate constants, calculated $Q_{e,cal}$ and experimental Q_e values for different initial dye concentrations, pH, and temperatures for the RB5 dye on the ECH-RB5 nanoparticles.

Parameters	Q_e	First-order kinetic model			Second-order kinetic model		
	(mg/g)(S.D.)	$k_1(\times10^{-3})$ (min^{-1})(S.D.)	$Q_{e,cal}$ (mg/g)(S.D.)	R^2 (mg/g)(S.D.)	$k_2(\times10^{-7})$ (g/mg min)(S.D.)	$Q_{e,cal}$ (mg/g)(S.D.)	R^2
Initial pH: 6.0 mg/mL initial dye concentration, 30 °C							
3.0	5057 (57)	1.17 (0.06)	2205 (7)	0.9233	1.77 (0.13)	4881 (168)	0.9995
4.0	4806 (58)	0. 97 (0.03)	2107 (80)	0.9222	1.52 (0.02)	4773 (322)	0.9996
6.0	3664 (120)	0. 86 (0.30)	1996 (48)	0.9257	1.40 (0.11)	3775 (100)	0.9987
Initial dye concentration (mg/mL): initial pH 3.0, 30 °C							
2.0	2125 (57)	0. 83 (0.04)	1634 (85)	0.9563	1.08 (0.08)	2274 (74)	0.9982
4.0	4355 (56)	0. 98 (0.14)	2742 (512)	0.923	1.46 (0.01)	4773 (322)	0.9983
6.0	5057 (57)	1.17 (0.06)	2205 (7)	0.9233	1.77 (0.13)	4881 (168)	0.9995
Temperature (°C): 6.0 mg/mL initial dye concentration, initial pH 3.0							
30	5057 (57)	1.17 (0.06)	2205 (7)	0.9233	1.77 (0.13)	4881 (168)	0.9995
40	5252 (103)	1.55 (0.43)	2159 (141)	0.8635	1.84 (0.18)	5588 (66)	0.9997
50	5587 (69)	1.82 (0.03)	2590 (17)	0.9305	1.86 (0.01)	5831 (72)	0.9996

Note: S.D. in the parentheses is the standard deviation.

Freundlich isotherm equation (8) [25],

$$\ln Q_e = b_F \ln C_e + \ln K_F, \tag{8}$$

and Dubinin-Radushkevich isotherm equation (9) [26],

$$\ln Q_e = K\varepsilon^2 + \ln Q_{DR}, \tag{9}$$

where C_e is the equilibrium concentration of the dye; Q_e is the adsorption capacity of the dye, Q_m, K_F, and Q_{DR} are the Langmuir; Freundlich and Dubinin-Radushkevich maximum adsorption capacities of the dye, respectively; K_L, b_F, and K are the Langmuir, Freundlich and Dubinin-Radushkevich constants, respectively; and ε is the Polanyi potential. The Polanyi potential (ε) is given as Eq. (10):

$$\varepsilon = RT \ln\left(1 + \frac{1}{C_e}\right) \tag{10}$$

where R is the gas constant in kJ/mol, and T is the temperate in Kelvin. The Dubinin-Radushkevich constant (K) can give the valuable information regarding the mean energy of adsorption by Eq. (11):

$$E = (-2K)^{-1/2} \tag{11}$$

Table 2
The first-order and second-order adsorption rate constants, calculated $Q_{e,cal}$ and experimental Q_e values for different initial dye concentrations, pH, and temperatures for the 3R dye on the ECH-3R nanoparticles.

Parameters	Q_e	First-order kinetic model			Second-order kinetic model		
	(mg/g)(S.D.)	$k_1(\times10^{-3})$ (min^{-1})(S.D.)	$Q_{e,cal}$ (mg/g)(S.D.)	R^2	$k_2(\times10^{-7})$ (g/mg min)(S.D.)	$Q_{e,cal}$ (mg/g)(S.D.)	R^2
Initial pH: 6.0 mg/mL initial dye concentration, 30 °C							
3.0	4811 (40)	0.99 (0.25)	2784 (209)	0.9244	5.99 (0.88)	5278 (393)	0.9993
4.0	4500 (15)	0. 80 (0.01)	3012 (77)	0.9710	6.10 (0.02)	4740 (32)	0.9980
6.0	3525 (13)	0. 89 (0.01)	2092 (52)	0.9574	8.68 (0.13)	3466 (25)	0.9959
Initial dye concentration (mg/mL): initial pH 3.0, 30 °C							
2.0	1994 (40)	0. 90 (0.01)	1175 (23)	0.9467	1.94 (0.23)	2086 (4)	0.9993
4.0	4130 (1)	0. 99 (0.03)	2374 (37)	0.9576	5.68 (0.88)	4033 (46)	0.9973
6.0	4811 (40)	0.99 (0.25)	2784 (209)	0.9244	5.99 (0.88)	5278 (393)	0.9993
Temperature (°C): 6.0 mg/mL initial dye concentration, initial pH 3.0							
30	4811 (40)	0.99 (0.25)	2784 (209)	0.9244	5.99 (0.88)	5278 (393)	0.9993
40	4909 (38)	0.98 (0.26)	2193 (141)	0.8520	7.00 (0.09)	5051 (72)	0.9993
50	5037 (10)	1.49 (0.44)	2471 (40)	0.9005	8.79 (0.61)	5000 (1)	0.9986

Note: S.D. in the parentheses is the standard deviation.

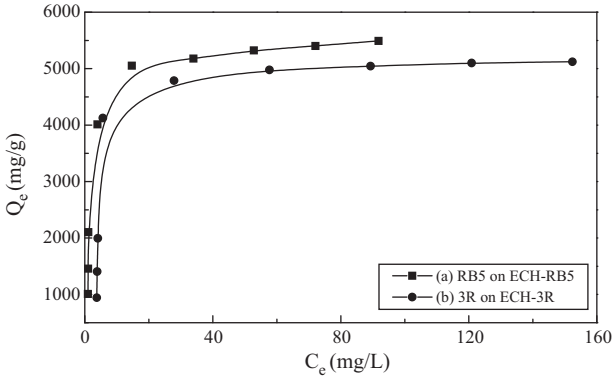

Fig. 9. Equilibrium adsorption of (a) the RB5 dye on the ECH-RB5 nanoparticles and (b) the 3R dye on the ECH-3R nanoparticles at initial pH 3.0 and at 30 °C for 120 h with different equilibrium dye concentrations.

where E is the mean adsorption energy, and K is the Dubinin-Radushkevich constant. According to Eq. (7), the plot of C_e/Q_e against C_e gives a straight line with a slope of $1/Q_m$ and an intercept of $1/(Q_mK_L)$. In Eq. (8), K_F and b_F can calculated from a linear plot of $\ln Q_e$ versus $\ln C_e$. In Eq. (9), the plot of $\ln Q_e$ versus ε^2 gives a straight line with a slope of K and an intercept of $\ln Q_{DR}$

The model parameters along with the correlation coefficients (R^2) and standard deviations obtained from the three isotherm models were listed in Table 3. The Langmuir adsorption model was found to sufficiently fit the experimental data of the RB5 dye on the ECH-RB5 nanoparticles and the 3R dye on the ECH-3R nanoparticles compared with the linear correlation coefficients. Moreover,

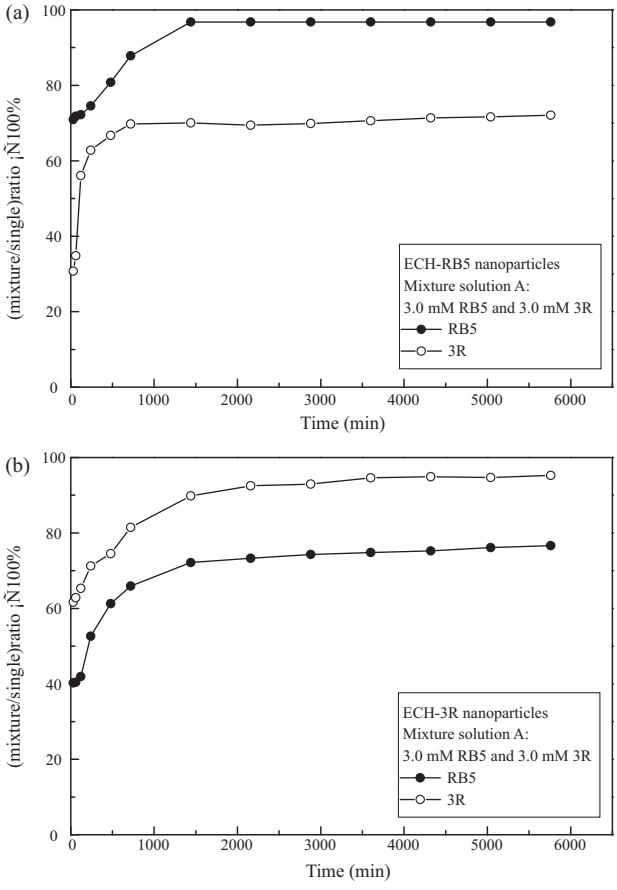

Fig. 10. The ratio of the adsorption capacity between the mixture solution A and the single dye solution on (a) the ECH-RB5 and (b) ECH-3R nanoparticles.

the mean adsorption energy (E) calculated from the Dubinnin-Radushkevich model may involve the transfer of the free energy of one mole of solute from infinity (in solution) to the surface of the adsorbent. The adsorption behavior can predict the physical adsorption in the range of 1–8 kJ/mol and the chemical adsorption in more than 8 kJ/mol [17,18]. The E values (13.02 and 11.23 kJ/mol, respectively) of the RB5 and 3R dyes indicated that the adsorption process may be due to the dual nature of the process, physisorption and chemisorption, and the fact that that adsorption was predominant in the chemisorption process.

The degrees of suitability of the nanoparticles of these two dyes were estimated from the separation factors (R_L) using Eq. (12) [16,27,28]:

$$R_L = \frac{1}{(1 + K_L C_i)} \tag{12}$$

where K_L is Langmuir constant and C_i is the initial concentration of dye.

The separation factor (R_L) with values between 0 and 1 reveals the suitability of the process. The values of R_L in the adsorption of the RB5 dye on the ECH-RB5 nanoparticles and the values of the 3R dye on the ECH-3R nanoparticles were between 0.0003 and 0.0044 and between 0.0020 and 0.0328, respectively, for all concentration ranges at 30, 40, and 50 °C. This indicated the suitability of the nanoparticles for the adsorption of the RB5 and 3R dyes.

Recently, Yilmaz and Memon reported on solvent extraction and adsorption of dyes and metals from aqueous solutions using calyx[n]arene derivatives [29–33]. They revealed that the extraction of the RB5 dye with calyx[4]arene derivatives was within the ranges of 1.0% to 11.8%, and adsorption of the RB5 dye by calyx[4]arene immobilized on the surface of modified Amberlite XAD-4 resin was approximately within the range of 30% to 60% [29,30]. The removal percentages of the RB5 and 3R dyes by the ECH-RB5 and ECH-3R nanoparticles were from 74% to 94% and from 72% to 87%, respectively. Table 4 listed the comparison of the maximum monolayer adsorption capacity (Q_m) of Remazol Black 5 and Remazol Brilliant Orange 3R dyes on various adsorbents. The data indicated that the maximum monolayer adsorption capacities (5572 and 5392 mg/g, respectively) of the RB5 dye on the ECH-RB5 nanoparticles and the 3R dye on the ECH-3R nanoparticles were greater than those of other adsorbents. Furthermore, they had 3.3 and 2.6 times of Q_m in the RB5 and 3R dyes on the GLA-crosslinked-chitosan microparticles (149–250 μm) prepared from homogeneous coupling and microparticle formation using NaOH solution, respectively [17]. In addition, they had 1.9 times of Q_m in the RB5 dye on the templated ECH-crosslinked-chitosan microparticles (149–250 μm) [18]. The technique used in this study offers a convenient and economical method for the preparation of templated nanoparticles, which can facilitate a higher adsorption capacity and thus a more efficient adsorption of dyes in an aqueous solution compared with nature or other synthetic materials.

3.4. Adsorption thermodynamics

The adsorption isotherm data obtained from different temperatures were used to calculate the thermodynamic parameters associated with the adsorption process. Based on the van't Hoff equation, Langmuir constants (K_L) were used to determine the standard Gibbs free energy change (ΔG°), standard enthalpy change (ΔH°), and standard entropy change (ΔS°), as shown in Eqs. (13) and (14) [15,16,23,28]:

$$\ln KL = -\frac{\Delta H^\circ}{RT} + \frac{\Delta S^\circ}{R} \tag{13}$$

$$\Delta G^\circ = \Delta H^\circ - T\Delta S^\circ \tag{14}$$

Table 3
Langmuir, Freundlich and Dubinin-Radushkevich isotherm parameters for the RB5 dye on the ECH-RB5 nanoparticles and the 3R dye on the ECH-3R nanoparticles at pH 3.0 and at 30 °C for 120 h.

Parameter	RB5 on ECH-RB5	3R on ECH-3R
Langmuir isotherm		
Q_m (mg/g) (S.D.)	5572 (66)	5392 (103)
K_L (L/mg) (S.D.)	0.2880 (0.0371)	0.1246(0.0030)
R^2	0.9991	0.9934
Freundlich isotherm		
K_F (mg/g) (S.D.)	2508 (22)	1138 (29)
b_F (S.D.)	0.1651 (0.0029)	0.3378(0.0010)
R^2	0.9066	0.6749
Dubinin-Radushkevich isotherm		
Q_{DR} (mg/g) (S.D.)	6004 (5)	5169 (143)
$K(\times 10^{-9}$ J^2/mol^2) (S.D.)	−0.160 (0.002)	−3.400 (0.150)
E (kJ/mol) (S.D.)	13.02 (0.11)	11.23 (0.27)
R^2	0.7698	0.7331

Note: S.D. in the parentheses is the standard deviation.

Table 4
Comparison of the maximum monolayer adsorption capacity (Q_m) of Remazol Black 5 and Remazol Brilliant Orange 3R dyes on various adsorbents.

Azo dye	Adsorbent (diameter) and method of preparation	Q_m (mg/g)	Reference
Remazol Black 5	ECH-RB5 nanoparticles (189–194 nm) homogeneous coupling, using TPP	5572	This work
	Chitosan/amino resin and chitosan bearing both amine and quaternary ammonium chloride moieties	625–932	[16]
	GLA-crosslinked-chitosan microparticles (149–250 μm), homogeneous coupling, using NaOH	1680	[17]
	Templated ECH-crosslinked chitosan (149–250 μm), homogeneous coupling, using NaOH	2941	[18]
	Acid-treated biomass microparticles (400–600 μm) of brown seaweed Laminaria sp.	102	[23]
Remazol Brilliant Orange 3R	ECH-3R nanoparticles (186–200 nm) homogeneous coupling, using TPP	5392	This work
	GLA-crosslinked quaternary chitosan microparticles (53–177 μm), heterogeneous coupling,	1060	[15]
	GLA-crosslinked-chitosan microparticles (149–250 μm), homogeneous coupling, using NaOH	2041	[17]

Note: The maximum monolayer adsorption capacity (Q_m) is obtained from Langmuir isotherm equation.

Table 5
The first-order and second-order rate constants and intraparticle diffusion parameters for different mixture solutions of the RB5 and 3R dyes on the ECH-RB5 nanoparticles at initial pH 3.0 and at 30 °C.

Mixture	First-order kinetic model		Second-order kinetic model		Intraparticle diffusion model		
	$k_1 \times 10^{-3}$ (S.D.)	R^2	$k_2 \times 10^{-3}$ (S.D.)	R^2	$k_{p,1}$ (S.D.)	$k_{p,2} \times 10^{-3}$ (S.D.)	$k_{p,3} \times 10^{-3}$ (S.D.)
Solution A (initial conc.: 3.0 mM RB5 and 3.0 mM 3R)							
RB5	0.99	0.9631	1.15	0.9863	0.052	11.29	2.87
	(0.01)		(0.01)		(0.001)	(0.11)	(0.03)
3R	0.82	0.9129	4.09	0.9990	0.068	18.30	3.67
	(0.16)		(0.10)		(0.001)	(0.04)	(1.66)
Solution B (initial conc.: 3.0 mM RB5 and 6.0 mM 3R)							
RB5	0.87	0.9464	0.69	0.9854	0.072	5.40	2.50
	(0.01)		(0.01)		(0.001)	(0.16)	(0.20)
3R	1.03	0.9873	0.93	0.9977	0.192	53.50	4.80
	(0.11)		(0.01)		(0.001)	(0.73)	(0.25)

Note: S.D. in the parentheses is the standard deviation. k_1 in min^{-1}, k_2 in g mmol^{-1} min^{-1}, and $k_{p,1}$, $k_{p,2}$ and $k_{p,3}$ in mmol g^{-1} min$^{-0.5}$.

Table 6
The first-order and second-order rate constants and intraparticle diffusion parameters for different mixture solutions of RB5 and 3R dyes on ECH-3R nanoparticles at initial pH 3.0 and at 30 °C.

Mixture	First-order kinetic model		Second-order kinetic model		Intraparticle diffusion model		
	$k_1 \times 10^{-3}$ (S.D.)	R^2	$k_2 \times 10^{-3}$ (S.D.)	R^2	$k_{p,1}$ (S.D.)	$k_{p,2} \times 10^{-3}$ (S.D.)	$k_{p,3} \times 10^{-3}$ (S.D.)
Solution A (initial conc.: 3.0 mM RB5 and 3.0 mM 3R)							
RB5	0.93	0.9150	1.39	0.9889	0.076	17.30	3.18
	(0.01)		(0.03)		(0.001)	(0.15)	(0.03)
3R	0.79	0.9645	2.35	0.9988	0.100	23.40	5.06
	(0.02)		(0.05)		(0.004)	(0.69)	(0.35)
Solution B (initial conc.: 3.0 mM RB5 and 6.0 mM 3R)							
RB5	0.91	0.9138	1.00	0.9864	0.055	6.80	3.55
	(0.01)		(0.01)		(0.001)	(0.30)	(0.40)
3R	0.90	0.9848	1.38	0.9984	0.161	43.20	9.51
	(0.01)		(0.62)		(0.001)	(0.39)	(0.08)

Note: S.D. in the parentheses is the standard deviation. k_1 in min^{-1}, k_2 in g mmol^{-1} min^{-1}, and $k_{p,1}$, $k_{p,2}$ and $k_{p,3}$ in mmol g^{-1} min$^{-0.5}$

The values of ΔH° and ΔS° can be calculated from the slope and intercept using the plotted graph of $\ln K_L$ versus $1/T$. The thermodynamic parameters for the adsorption of the RB5 dye on the ECH-RB5 nanoparticles and the 3R dye on the ECH-3R nanoparticles were determined. The negative values of ΔG° (−32.09, −33.77 and −34.63 kJ/mol for the RB5 dye and −28.17, −28.83 and −29.50 kJ/mol for the 3R dye at 30, 40 and 50 °C, respectively) and ΔH° (−6.77 and −8.05 kJ/mol for the RB5 and 3R dyes, respectively) showed that the adsorption processes on the nanoparticles were spontaneous and exothermic. On the other hand, the positive values of ΔS° (86.27 and 87.11 J/mol K for the RB5 and 3R dyes, respectively) increased the randomness during the adsorption of these two dyes on the nanoparticles. This may arise from liberation of water molecules from the hydrated shells of the adsorbed species [16].

3.5. Competition adsorption

The kinetics of the competition adsorption of the single solution and mixture solution A (3.0 mM initial concentration of each dye) of the RB5 and 3R dyes on the ECH-RB5 and ECH-3R nanoparticles, respectively, was studied with a pH of 3.0 and a temperature of 30 °C. The initial adsorption rate of the RB5 dye on the ECH-RB5 nanoparticles in mixture solution A was faster than that of the 3R dye. However, the initial adsorption of the RB5 dye on the ECH-3R nanoparticles in mixture solution A was slower than that of the 3R dye. This may be ascribed to the fact that the ECH-RB5 nanoparticles have more suitable sites for the adsorption of RB5 molecules than ECH-3R nanoparticles. Fig. 10(a) and (b) showed the ratio of adsorption capacity of each dye between mixture solution A and each single solution with the same initial concentration of each dye. The ECH-RB5 nanoparticles revealed that the ratio of the RB5 dye remained at 99%, whereas that of the 3R dye appeared to be only 72%. On the other hand, the ECH-3R nanoparticles showed that the ratio of the 3R dye also remained at 95%, whereas that of the RB5 dye was only 69%.

To study the competition adsorption in a mixture with a higher concentration of the 3R dye, mixture solution B, a mixture with an initial 3R dye of 6.0 mM and an RB5 dye of 3.0 mM, was used. The kinetics of the competition adsorption of the RB5 and 3R dyes on the ECH-RB5 and ECH-3R nanoparticles in mixture solution B had a pH of 3.0 and a temperature of 30 °C. The adsorption rates of the 3R dye on the ECH-RB5 and ECH-3R nanoparticles were significantly faster than that of the RB5 dye. As the 3R dye contained a higher initial molar concentration, it resulted in a stronger driving force in the adsorption process [13]. Fig. 11(a) and (b) shows the ratio of the adsorption capacity of each dye in mixture solution B and in each single solution. The ratio of the 3R dye on the ECH-RB5 and ECH-3R nanoparticles remained at 90%, whereas that of the RB5 dye was less than 70%. This indicates that the adsorption of the 3R dye on both nanoparticles in mixture solution B, the solution with a higher initial concentration of the 3R dye, is much less affected by the existence of the RB5 dye than the other way around in competitive adsorption.

Tables 5 and 6 showed the analysis of the adsorption rate of the RB5 and 3R dyes on the ECH-RB5 and ECH-3R nanoparticles, respectively, using the first-order and second-order kinetic models for mixture solutions A and B. A comparison of the linear correlation coefficients (R^2) listed in Tables 5 and 6 showed that the second-order kinetic model fitted well and was better than the first-order model for mixture solutions A and B.

3.6. Intraparticle diffusion model

The intraparticle diffusion model was applied to study the competition adsorption of the RB5 and 3R dyes in mixture solutions A and B. The intraparticle diffusion equation is described as Eq. (15) [34]:

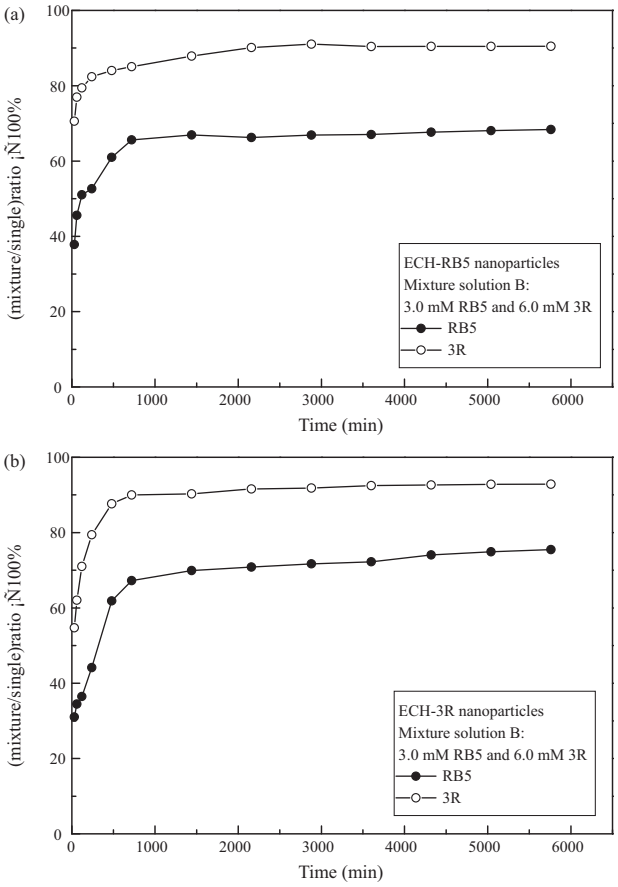

Fig. 11. The ratio of the adsorption capacity between the mixture solution B and the single dye solution for (a) the ECH-RB5 and (b) ECH-3R nanoparticles.

$$Q_t = k_i t^{0.5} + C \quad (15)$$

where k_i, Q_t, and C are intraparticle diffusion rate constant, adsorption capacity of dye at a given time t and a constant, respectively. k_i is the slope of the straight-line portions of the plot of Q_t versus the square root of time ($t^{0.5}$). As shown in Fig. 12(a) and (b), multilinearities were observed through the plot of Q_t versus $t^{0.5}$, for the competition adsorption of the RB5 and 3R dyes on the ECH-RB5 and ECH-3R nanoparticles, respectively, in mixture solutions A and B. This indicates that three steps were undertaken in the adsorption processes [13,35]. The first sharper portion is the mass transfer of solute molecules from the bulk solution to the adsorbent surface; this is also known as instantaneous adsorption. The second portion is the gradual adsorption stage, wherein intraparticle diffusion is rate limiting. The third portion is the final equilibrium stage, wherein intraparticle diffusion starts to slow down due to the extremely low solute concentration in the solution. According to Fig. 12(a) and (b), the slope of the line in each stage was indicated as the rate parameter $k_{p,i}$ (i = 1–3). In Tables 5 and 6, the data showed that the order of the adsorption rate was $k_{p,1} > k_{p,2} > k_{p,3}$ for each dye on both nanoparticles in mixture solutions A and B. Furthermore, in mixture solution A, the mixture with equal initial dye concentrations, the values of $k_{p,2}$ for the 3R dye on the ECH-RB5 and ECH-3R nanoparticles were 1.6 and 1.4 times more than those for the RB5 dye, respectively. This is attributed to the fact that the 3R molecule is smaller and diffuses faster than the RB5 molecule. However, in mixture solution B, the mixture in which the initial concentration of the 3R dye was twice that of the RB5 dye, the val-

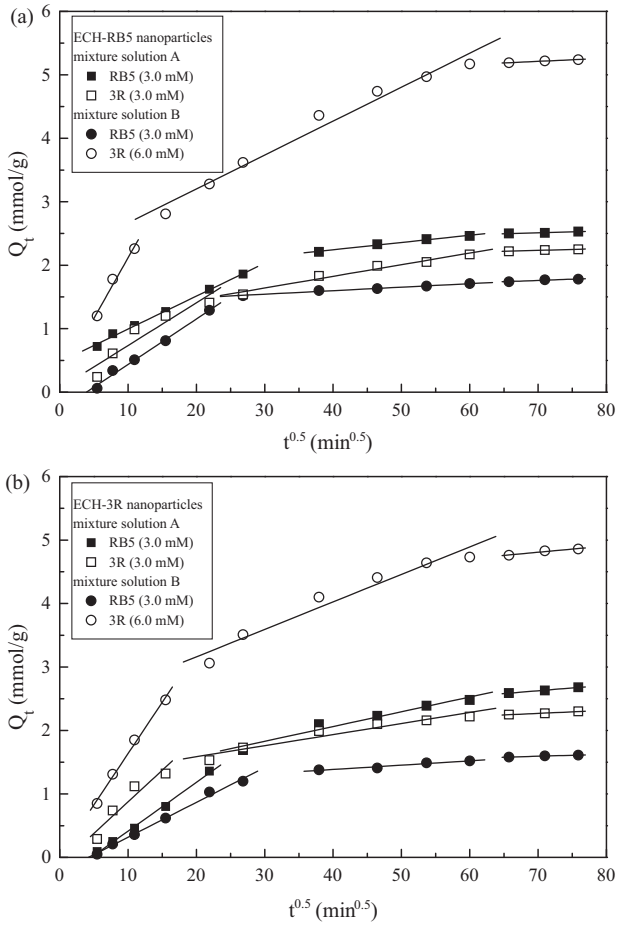

Fig. 12. The intraparticle diffusion kinetics for the RB5 and 3R dyes on (a) the ECH-RB5 and (b) the ECH-3R nanoparticles in the mixture solutions A and B at initial pH 3.0 and 30 °C.

ues of $k_{p,2}$ for the 3R dye in the ECH-RB5 and ECH-3R nanoparticles were 9.9 and 6.4 times more than those for the RB5 dye, respectively. This is not only caused by the influence of molecular size but also by the effect of initial dye concentration [13]. This showed that competition adsorption apparently favors the 3R dye on both nanoparticles in mixture solution B.

3.7. Regeneration

The adsorption capacities of the RB5 dye on the ECH-RB5 nanoparticles and the 3R dye on the ECH-3R nanoparticles in the adsorption, desorption, and adsorption steps were shown in Fig. 13. The adsorption condition was set to 6.0 mg/mL initial dye concentration, with an initial pH of 3.0, and a temperature of 30 °C, whereas the desorption condition had an initial pH of 14.0 of the NaOH solution and a temperature of 30 °C. The first adsorption step lasted for 96 h, and the adsorption capacities of the RB5 dye on the ECH-RB5 nanoparticles and the 3R dye on the ECH-3R nanoparticles reached the value of 5077 and 4845 mg/g, respectively. The desorption step for 96 h removed 78% and 79% of the RB5 dye on the ECH-RB5 nanoparticles and the 3R dye on the ECH-3R nanoparticles, respectively. This may be due to the fact that in a basic solution, the positively charged amino groups are deprotonated, and the electrostatic interaction between chitosan and dye molecules becomes much weaker [11,17]. At the same time, the adsorption of the RB5 and 3R dyes on the nanoparticles may be attributed to the dual nature of the process, physisorption and chemisorption, which results in incomplete desorption [11,17]. The

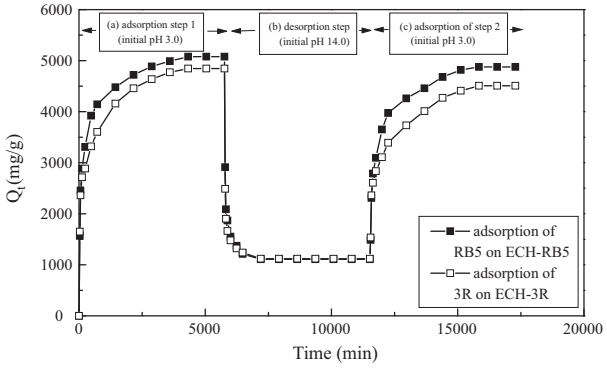

Fig. 13. Adsorption and desorption of the RB5 dye on the ECH-RB5 nanoparticles and the 3R dye on the ECH-3R nanoparticles at 6.0 mg/mL initial dye concentration and 30 °C with three steps: adsorption step 1 at initial pH 3.0, desorption step at initial pH 14.0 and adsorption step 2 at initial pH 3.0.

second adsorption step that lasted for 96 h adsorbed again 74% and 70% of the RB5 dye in the ECH-RB5 nanoparticles and the 3R dye in the ECH-3R nanoparticles at the first adsorption step, respectively. Thus, the nanoparticles were regenerated and reutilized for further dye adsorption.

4. Conclusion

The nanoparticles of the templated crosslinked chitosan, ECH-RB5 and ECH-3R, were prepared through the imprinting process with the RB5 or 3R dyes as templates, respectively, and with ECH as a crosslinker. The maximum monolayer adsorption capacities of the RB5 dye on the ECH-RB5 nanoparticles and the 3R dye on the ECH-3R nanoparticles were greater than those of other adsorbents reported in related studies. The adsorption experiments were in accordance with the second-order adsorption and the Langmuir adsorption models. Meanwhile, the *E* values of the RB5 and 3R dyes calculated using the Dubinnin-Radushkevich model revealed that the adsorption process may be attributed to the dual nature of the process, physisorption and chemisorption, and the fact that adsorption was predominant in the chemisorption process. In addition, the adsorption processes on the nanoparticles were spontaneous and exothermic. The competition adsorption through the analysis of the intraparticle diffusion model apparently favored the 3R dye more than the RB5 dye in the nanoparticles in mixture solution B. The adsorption of the dyes on the nanoparticles can be desorbed efficiently using alkaline solution, and the nanoparticles can be recycled for dye removal. The technique used in this study offers a convenient and economical method for the preparation of templated nanoparticles, which can facilitate a higher adsorption capacity and thus a more efficient adsorption of dyes in an aqueous solution compared with nature or other synthetic materials.

Acknowledgement

The authors gratefully acknowledge financial support from Southern Taiwan University.

References

[1] G. Crini, P.M. Badot, Application of chitosan, a natural aminopolysaccharide, for dye removal from aqueous solutions by adsorption processes using bath studies: a review of recent literature, Prog. Polym. Sci. 33 (2008) 399–447.
[2] I.T. Peternel, N. Koprivanac, A.M.L. Bozic, H.M. Kusic, Comparative study of UV/TiO_2, UV/ZnO and photo-Fenton processes for the organic reactive dye degradation in aqueous solution, J. Hazard. Mater. 148 (2007) 477–484.
[3] B. Volesky, Biosorption and me, Water Res. 41 (2007) 4017–4029.
[4] Z.G. Hu, J. Zhang, W.L. Chan, Y.S. Szeto, The sorption of acid dye onto chitosan nanoparticles, Polymer 47 (2006) 5838–5842.

[5] E. Guibal, L. Dambies, C. Milot, J. Roussy, Influence of polymer structural parameters and experimental conditions on metal anion sorption by chitosan, Polym. Int. 48 (1999) 671–680.
[6] H. Yoshida, S. Fukuda, A. Okamoto, T. Ktaoka, Recovery of direct dye and acid dye by adsorption on chitosan fiber-equilibria, Water Sci. Technol. 23 (1991) 1667–1676.
[7] F.C. Wu, R.L. Tseng, R.S. Juang, Comparative adsorption of metal and dye on flake- and bead-types of chitosan prepared from fishery wastes, J. Hazard. Mater. B73 (2000) 63–75.
[8] F.C. Wu, R.L. Tseng, R.S. Juang, Enhanced abilities of highly swollen chitosan beads for color removal and tyrosinase immobilization, J. Hazard. Mater. B81 (2001) 167–177.
[9] S. Chatterjee, S. Chatterjee, B.P. Chatterjee, A.R. Das, A.K. Guha, Adsorption of a model anionic dye, ecosin Y, from aqueous solution by chitosan hydrobeads, J. Colloid Interface Sci. 288 (2005) 30–35.
[10] M.S. Chiou, H.Y. Li, Equilibrium and kinetic modeling of adsorption of reactive dye on crosslinked chitosan beads, J. Hazard. Mater. B93 (2002) 233–248.
[11] M.S. Chiou, H.Y. Li, Adsorption behavior of reactive dye in aqueous solution on chemical cross-linked chitosan beads, Chemosphere 50 (2003) 1095–1105.
[12] M.S. Chiou, P.Y. Ho, H.Y. Li, Adsorption of anionic dyes in acid solutions using chemically cross-linked chitosan beads, Dyes Pigments 60 (2004) 69–84.
[13] M.S. Chiou, G.S. Chuang, Competitive adsorption of dye metanil yellow and RB15 in acid solution on chemically cross-linked chitosan beads, Chemosphere 62 (2006) 731–740.
[14] W.L. Du, R. Xu, X.Y. Han, Y.L. Xu, Z.G. Miao, Preparation, characterization and adsorption properties of chitosan nanoparticles for eosin Y as a model anionic dye, J. Hazard. Mater. 153 (2008) 152–156.
[15] S. Rosa, M.C.M. Laranjeira, H.G. Riela, V.T. Favere, Cross-linked quaternary chitosan as an adsorbent for the removal of the reactive dye from aqueous solutions, J. Hazard. Mater. 155 (2008) 253–260.
[16] K.Z. Elwakeel, Removal of Reactive Black 5 from aqueous solutions using magnetic chitosan resins, J. Hazard. Mater. 163 (2009) 382–392.
[17] A.H. Chen, S.M. Chen, Biosorption of azo dyes from aqueous solution by glutaraldehyde-crosslinked chitosans, J. Hazard. Mater. 172 (2009) 1111–1121.
[18] A.H. Chen, Y.Y. Huang, Adsorption of Remazol Black 5 from aqueous solution by the templated crosslinked-chitosans, J. Hazard. Mater. 177 (2010) 675–688.
[19] A. Baxter, M. Dillon, K.D.A. Taylor, Improved method for i.r. determination of the degree of N-acetylation of chitosan, Int. J. Biol. Macromol. 14 (1992) 166–169.
[20] G.A.F. Roberts, J.G. Domszy, Determination of the viscometric constants for chitosan, Int. J. Biol. Macromol. 4 (1982) 374–377.
[21] M.R. de Moura, F.A. Aouada, R.J. Avena-Bustillos, T.H. McHugh, J.M. Krochta, L.H.C. Mattoso, Improved barrier and mechanical properties of novel hydroxypropyl methylcellulose edible films with chitosan/tripolyphosphate nanoparticles, J. Food Eng. 92 (2009) 448–453.
[22] H. Yoshida, A. Okamoto, T. Kataoka, Adsorption of acid dye on crosslinked chitosan fibers: equilibria, Chem. Eng. J. 48 (1993) 2267–2272.
[23] K. Vijayaraghavan, Y.S. Yun, Biosorption of C.I. Reactive Black 5 from aqueous solution using acid-treated biomass of brown seaweed Laminaria sp., Dyes Pigments 76 (2008) 726–732.
[24] I. Langumuir, The adsorption of gases on plane surfaces of glass, mica and platinum, J. Am. Chem. Soc. 40 (1918) 1361–1403.
[25] H.M.F. Freundlich, Over the adsorption in solution, Z. Physik. Chem. A57 (1906) 358–471.
[26] S.P. Ramnani, S. Sabharwal, Adsorption behavior of Cr(VI) onto radiation crosslinked chitosan and its possible application for the treatment of wastewater containing Cr(VI), React. Funct. Polym. 66 (2006) 902–909.
[27] L. Qi, Z. Xu, Lead sorption from aqueous solutions on chitosan nanoparticles, Colloids Surf. A 251 (2004) 183–190.
[28] A.M. Donia, A.A. Atia, K.Z. Elwakeel, Selective separation of mercury(II) using magnetic chitosan resin modified with Schiff's base derived from thiourea and glutaldehyde, J. Hazard. Mater. 151 (2008) 372–379.
[29] O. Gungor, S. Memon, A. Yilmaz, M. Yilmaz, Evaluation of the performance of calix[n]arene derivatives as liquid phase extraction material for the removal of azo dyes, J. Hazard. Mater. 158 (2008) 202–207.
[30] M.A. Kamboh, I.B. Solangi, S.T.H. Sherazi, S. Memon, Synthesis and application of calix[4]arene based resin for the removal of azo-dyes, J. Hazard. Mater. 172 (2009) 234–239.
[31] I.B. Solangi, S. Memon, M.I. Bhanger, Synthesis and application of a highly efficient tetraestercalix[4]arene resin for the removal of Pb2+ from aqueous environment Anal, Chim. Acta 638 (2009) 146–153.
[32] I. Qureshi, S. Memon, M. Yilmaz, Estimation of chromium(VI) adsorption efficiency of novel regenerable p-tert-butylcalix[8]areneoctamide impregnated Amberlite XAD-4 Resin, J. Hazard. Mater. 164 (2009) 675–682.
[33] D.M. Roundhill, I.B. Solangi, S. Memon, M. Yilmaz, The liquid–liquid extraction of toxic metals (Cd, Hg and Pb) by calixarenes, Pak. J. Anal. Environ. Chem. 10 (2009) 1–13.
[34] B.H. Hameed, A.A. Ahmad, N. Aziz, Isotherms, kinetics and thermodynamics of acid dye adsorption on activated palm ash, Chem. Eng. J. 133 (2007) 195–203.
[35] W.H. Cheung, Y.S. Szeto, G. McKay, Intraparticle diffusion processes during acid dye adsorption onto chitosan, Bioresour. Technol. 98 (2007) 2897–2904.